Convection Parametrization

Peter Bechtold

ECMWF, Shinfield Park, Reading, UK
Peter.Bechtold@ecmwf.int

1. Introduction

More than 40 years have now passed since the pioneering work by Manabe and Stricker (1964), Kuo (1965), and Ooyama (1971) who first recognized the need to include some kind of convective parameterization in numerical models in order to represent 'subgrid' convective activity, and to avoid grid-scale saturated ascents that could quickly lead to numerical instability (see also Arakawa (2004) for a review on 'past present and future of cumulus parameterization').

At that time the horizontal grid resolution of global models was of *O*(400 km). Nowadays the horizontal resolution of global Numerical Weather Prediction models (NWPs) is of *O*(40 km) - in the ECMWF Integrated Forecasting System (IFS) it is 25 km since February 2006, and will reach resolutions of 15 km in 2009. Current and next generation limited area versions of NWPs will use horizontal resolutions of *O*(1-3 km), and therefore can resolve part of the motion spectrum associated to deep convection.

The reader might wonder if it is still necessary to learn about and to use 'traditional' convective parameterization. Our answer is Yes, first of all, it is and will be in the next 10-20 years still too costly to run medium range (global) weather prediction and assimilation systems at resolutions that allow for an explicit representation for deep convection. The same applies to seasonal and climate predictions. Second, even Cloud Resolving Models (CRMs) still require parameterization schemes for shallow convection as shallow convective clouds have typical radius of *O*(100 m). Third, it has not yet been proven that higher horizontal resolution and explicit representation of convection produces better medium range forecasts than current forecasts using classical convection parameterizations. E.g. it has already been recognized by Bjerknes (1938) using the famous 'slice method' that convection tends to prefer the smallest (resolvable) scales, and higher resolution means more small-scale 'noise' and uncertainty in the forecasts (in this case ensemble forecasts with an increased number of ensemble members would be necessary, further increasing the numerical burden). Classical convection parameterizations do generally efficiently stabilize the atmosphere and damp numerical noise. And last, but not least, classical convective parameterization schemes allow to 'understand' or 'constrain' atmospheric convection in some easy manner; learning about these concepts and schemes is instructive and constitutes a good exercise in physics and numerics.

We do not attempt to give an overview of convection parametrization and its theoretical background here. On this, the reader might find helpful information and an exhaustive reference list in Lecture Notes by Bechtold (2008). Rather, we want to place the convection problem in the context of global NWP, starting with the importance of subgrid physical parametrizations for the global energy cycle. Also discussed are a few convection parametrization 'methods' and 'tricks' that proofed to be robust and beneficial for the IFS. Practical applications including tracer transport, as well as short-range and seasonal forecasts of rain and clouds at various horizontal resolutions, and comparison with observational data and CRMs document the performance and limits of convection forecasts. We conclude with a discussion on the perspectives of convection parametrization including current research work.

2. Subgrid Physics and the global Lorenz energy cycle

Following Lorenz (1955) and Steinheimer et al. (2008) the production and generation of available potential energy (APE) in the atmosphere can be written as

$$\frac{da}{dt} = NQ + \alpha\omega = N\bar{Q} + \bar{\alpha}\bar{\omega} + \overline{\alpha'\omega'} \tag{1}$$

where NQ represents the generation rate of APE, with N the Lorenz efficiency factor that measures the efficiency of the atmospheric heat engine with respect to a barotropic reference state. Q is the net heating and is obtained from the models temperature equation[1]. As the temperature equation is based on the conservation of enthalpy, the net heating also contains the dissipation of kinetic energy.

The conversion rate of APE into kinetic energy = motion is given by $\alpha\omega$, with $\alpha=1/\rho$, ρ is density, and ω the vertical velocity (Pa/s). The latter term can be split in a grid-scale contribution that is contained in the model equations, and a subgrid-scale contribution that is not contained in the model equations. However, the subgrid-scale conversion rates can be computed from the convective and diffusive heat and moisture fluxes

$$\overline{\alpha'\omega'} = \frac{R}{P}[1 + (\varepsilon^{-1} - 1)]\,\overline{T'\omega'} + (\varepsilon^{-1} - 1)\bar{\alpha}\overline{q'\omega'} \tag{2}$$

with R the gaz constant for dry air, P pressure, q specific humidity, and ε=0.62 the ratio of the gas constants for dray air and water vapour.

The different generation and conversion terms have been computed with the aid of the IFS using 1-year integrations at resolution T159 and short-range integrations at resolution T511. The typical subgrid-scale conversion rates due to convection and diffusion are illustrated in Figure 1a. Convection dominates the free troposphere, and its contribution is important as it is (nearly) always positive, whereas diffusion dominates in the lowest 50 hPa. The grid-scale contributions (Figure 1b) are large, but can have both positive and negative sign so that globally there is a lot of cancellation. The radiation does not contribute to the conversion rates, but to the generation rates. Though even there its contribution is globally negative as e.g. given in the tropics, it is cooling in warm regions. However, the radiation heats the surface, and the surface heat and moisture fluxes contribute to the generation and conversion rates.

This leads us to the following energy diagram (Figure 2). One realises that the grid and subgrid generation and conversion rates are of similar magnitude with the grid-scale generation rate amounting to 3 W/m2 and the subgrid generation rate to 2.1 W/m2. The grid-scale conversion amounts to 3.4 W/m2 and the subgrid conversion rate to 1.7 W/m2. The total actual dissipation rate of the atmosphere would therefore be of about 5 W/m2. However, as the model equations do not include a subgrid conversion rate the actual dissipation rate of the model is equal to the gridscale conversion rate, and therefore amounts to 3.4 W/m2. And these 3.4 W/m2 are made up of surface dissipation and gravity wave drag (2.3 W/m2), convective momentum transport (0.4 W/m2), interpolation errors in the semi-Lagrangian advection scheme (0.5 W/m2), and horizontal diffusion (0.2 W/m2). The energy diagram highlights the importance of subgrid physical processes, and in particular the convective and diffusive contributions as well as the numerical aspects to the atmospheric motions. Therefore, progress in these areas should also lead to progress in the simulation of atmospheric activity and variability.

[1] http://www/ecmwf.int/research/ifsdocs/CY31r1/DYNAMICS/IFSPart3.pdf

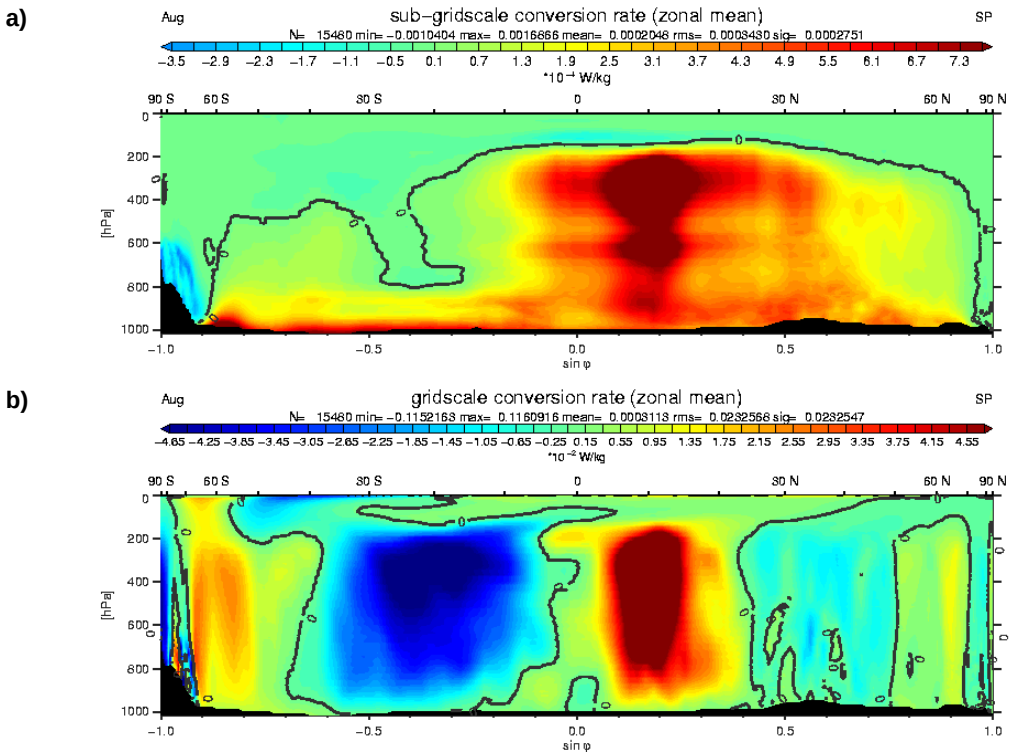

Figure 1. Zonal mean conversion rates (W/kg) of APE into kinetic energy for the month of August due to subgrid processes (convection and diffusion) (a), and the grid-scale conversion rates (b).

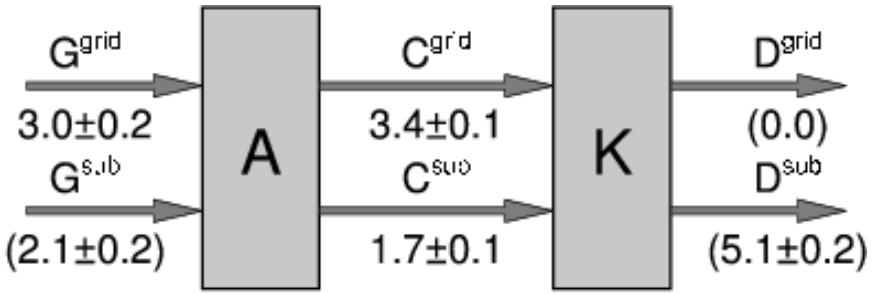

Figure 2. Lorenz type energy diagram including grid- and subgrid generation (G) rates of APE (A), and conversion (C) rates into kinetic energy (K), the latter being dissipated at rate D. All units are W/m2.

3. Convective tendencies and the mass flux approximation

Convection implies motions that are highly variable in space and time. It is therefore difficult to 'measure' convection. However, one can measure, and also parameterize, the ensemble effect of the convective motions on the large-scale. Following Yanai et al. (1973) the ensemble or bulk effect of convection on the large-scale can be conveniently derived from the basic equations of motion in pressure coordinates using the dry static energy $s = c_p T + gz$, and specific humidity q, with c_p the specific heat of dry air and L the latent heat of vaporisation/sublimation.

$$
\begin{aligned}
Q_{1c} &\equiv L(\overline{c}-\overline{e}) - \frac{\partial \overline{\omega' s'}}{\partial p} = L(\overline{c}-\overline{e}) + g\frac{\partial\left[M^c(s^c-\overline{s})\right]}{\partial p} \\
Q_2 &\equiv -L(\overline{c}-\overline{e}) - L\frac{\partial \overline{\omega' q'}}{\partial p} = -L(\overline{c}-\overline{e}) + Lg\frac{\partial\left[M^c(q^c-\overline{q})\right]}{\partial p} \\
Q_3 &\equiv -\frac{\partial \overline{\omega' \vec{v}_h'}}{\partial p} = g\frac{\partial\left[M^c(\vec{v}^c-\overline{\vec{v}})\right]}{\partial p}
\end{aligned}
\tag{3}
$$

where Q_1 is the convective apparent heat source, Q_2 the moisture sink, Q_3 the convective momentum tendency (with a similar equation holding for tracer transport), and c-e is condensation-evaporation. On the rhs of (3) the mass flux approximation has been applied to the transport term using a formal cloud/environment decomposition, with superscript c denoting average incloud values, and $M^c = M^u + M^d$ the convective mass flux (superscripts u and d denote the updraught/downdraught decomposition as actually applied in the model). The heat source is dominated by the net condensation term, whereas for moisture the transport and net condensation terms are equally important. Transport is the only process for momentum and tracers (if one neglects washout effects for the latter). To predict the influence of convection on the large-scale with this approach one first needs to determine where convection occurs and then compute the convective mass-flux, the values of the thermodynamic (and momentum) variables inside the convective elements and the condensation/evaporation term. This requires, as usual, a cloud model and a closure to determine the absolute (scaled) value of the mass flux as illustrated in Figure 3 (for a demonstration on the 'parametrizability' of deep convection the reader is referred to Gregory and Miller (1987)).

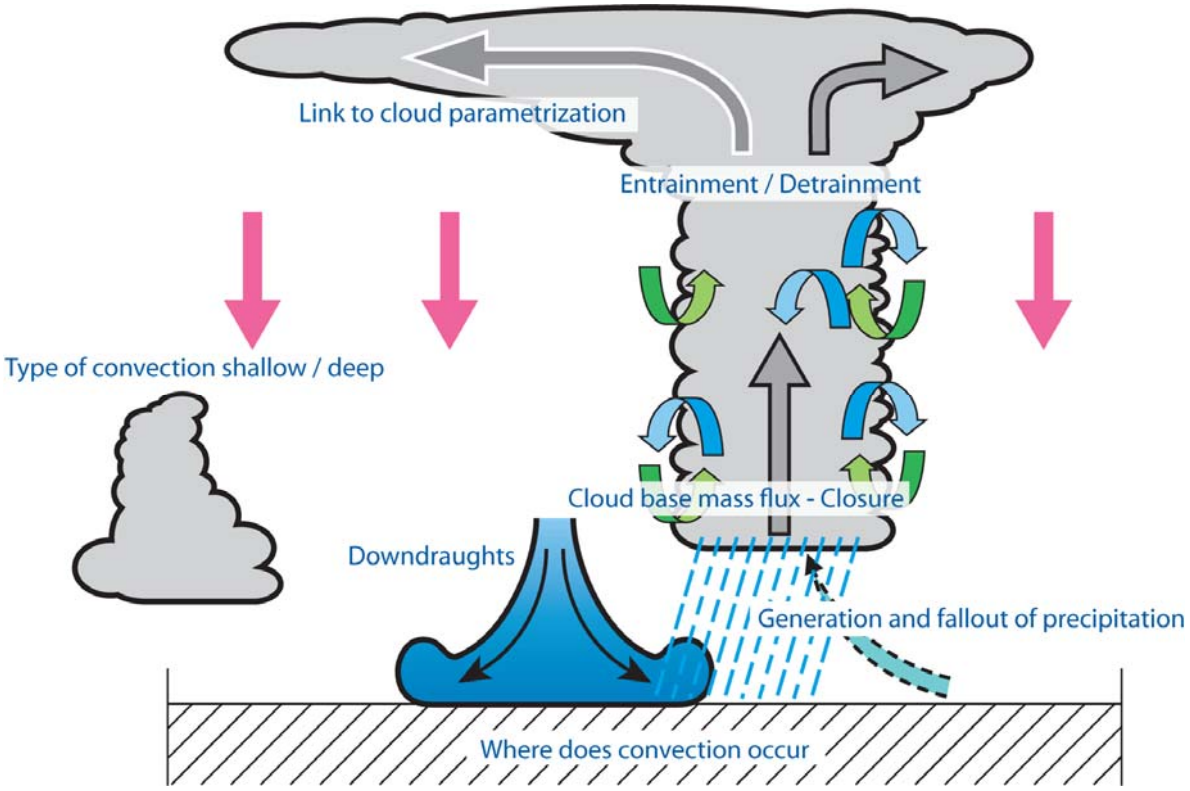

Figure 3. Schematic of a bulk convection scheme with a shallow and deep entraining/detraining cloudy ascending plume, and downdraught region. Further represented features are trigger of convection, environmental subsidence, microphysics and precipitation, and detrainment of cloud mass in anvils.

3.1. Entrainment and Detrainment

The exchange of mass between the cloud and the environment is formulated using fractional entrainment ε and detrainment rates δ

$$\frac{1}{M^c}\frac{\partial M^c}{\partial z} = \varepsilon - \delta = \varepsilon_{turb} + \varepsilon_{org} - \delta_{turb} - \delta_{org} \tag{4}$$

Unfortunately, the entrainment/detrainment rates are not known and can be highly variable in space and time (e.g. Lin and Arakawa, 1997). This is the weakest part of a (mass flux) convection parametrization, as simply taking constant entrainment rates does not produce satisfactory results in a global model, and also does not reproduce the observed sensitivity of convection to environmental humidity (Redelsperger et al., 2002; Derbyshire, 2004). Taking a multi-plume approach where each convective plume has different (but constant) entrainment/detrainment rates as done in Arakawa and Schubert (1974) also doesn't really solve the problem, as the plume ensemble is dominated by the least entraining parcel.

A pragmatic approach has been taken in the IFS. The entrainment is specified as the sum of a constant 'turbulent' part, and an 'organized' entrainment, active when the parcel is positively buoyant, that depends on the relative humidity of the environment. The formulation is scaled by a function rapidly decreasing with height, mimicking a cloud ensemble. Therefore, if the turbulent detrainment is taken constant, from a given height the detrainment rate will exceed the entrainment rate and the mass flux starts to decrease with height.

$$\begin{aligned} \varepsilon &= \underbrace{c_0}_{turb} F_{\varepsilon,1} + \underbrace{c_1 \frac{\overline{q}_s - \overline{q}}{\overline{q}_s}}_{org,\,buoy>0,\,deep\ only} F_{\varepsilon,2}; \quad F_{\varepsilon,i} = \left(\frac{\overline{q}_s}{\overline{q}_{s\,base}} \right)^{\beta_i}; \beta_1 = 2, \beta_2 = 3 \\ c_0; c_1; c_2 &= O(10^{-4} - 10^{-3} m^{-1}); \end{aligned} \tag{5}$$

Organized detrainment is active when negative buoyancy occurs. It is then set equal to the change in updraught kinetic energy with height. The above formulation has been successful in representing a realistic climatology of the model, as well as realistic tropical wave and intraseasonal variability (Bechtold et al. 2008) (see also Seminar paper by T. Jung).

3.2. Closure for deep convection

Most mass flux deep convection schemes employ some type of CAPE (Convective Available Potential Energy) closure which assumes that deep convection reduces CAPE to zero over a time scale τ. However, the quantity required by the parameterization is the cloud base mass flux. A simple and numerically efficient method to relate CAPE to the cloud base mass flux is given as follows. Recall that the definition of CAPE is

$$CAPE = \int_{base}^{top} g \frac{\theta_v^c - \overline{\theta}_v}{\overline{\theta}_v} dz \tag{6}$$

Taking the time derivative of (6) , assuming stationary cloud boundaries, gives

$$\left(\frac{\partial CAPE}{\partial t} \right)_{cu} = g \int_{base}^{top} \frac{\overline{\theta}_v \frac{\partial \theta_v^c}{\partial t} - \theta_v^c \frac{\partial \overline{\theta}_v}{\partial t}}{\overline{\theta}_v^{\,2}} dz \tag{7}$$

As we assume a stationary cloud $\frac{\partial \theta_v^c}{\partial t} = 0$; furthermore, $\frac{\theta_v^c}{\overline{\theta}_v} \approx 1$ so that (7) can be simplified to

$$\left(\frac{\partial CAPE}{\partial t}\right)_{cu} = -g \int_{cloud} \frac{1}{\overline{\theta}_v}\left(\frac{\partial \overline{\theta}_v}{\partial t}\right)_{cu} dz \tag{8}$$

Now, in order to make appear the mass flux, the environmental tendency of θ_v is expressed with the aid of the mass flux formulation in its truncated advective form derived from (3)a

$$\left(\frac{\partial \overline{\theta}_v}{\partial t}\right)_{cu} = -gM^c \frac{\partial \overline{\theta}_v}{\partial p} + \delta \frac{M^c}{\overline{\rho}} (\theta_v^u - \overline{\theta_v}) \approx \frac{M^c}{\overline{\rho}} \frac{\partial \overline{\theta}_v}{\partial z}, \tag{9}$$

where only the environmental compensating subsidence term has been retained. Reporting (9) into (8) and simplifying the time derivative gives

$$\left(\frac{\partial CAPE}{\partial t}\right)_{cu} = -g \int_{base}^{top} \frac{M^c}{\overline{\rho}\overline{\theta}_v} \frac{\partial \overline{\theta}_v}{\partial z} dz = -\frac{CAPE}{\tau}. \tag{10}$$

As the downdraught mass flux is proportional to the updraught mass flux, and mass fluxes at each level can be expressed as the product of the cloud base mass flux times a vertical function, it is possible to write

$$M^c = M^u + M^d = M_b^u \eta^u + M_t^d \eta^d = M_b^u (\eta^u - \alpha \eta^d); \quad M^d = -\alpha M^u, \tag{11}$$

and the final result is

$$M_{u,b}^n = \frac{\frac{CAPE}{\tau}}{g \int_{cloud} \left(\eta^u - \alpha \eta^d\right) \frac{1}{\rho \overline{\theta}_v} \frac{\partial \overline{\theta}_v}{\partial z} dz} = \frac{\frac{CAPE}{\tau}}{g \int_{cloud} \frac{M_c^{n-1}}{M_{u,b}^{n-1}} \frac{1}{\rho \overline{\theta}_v} \frac{\partial \overline{\theta}_v}{\partial z} dz}. \tag{12}$$

where an iteration index *n* has been introduced. The solution of (12) requires a 'first guess' mass flux profile M_c^{n-1} with together with the CAPE is obtained from a first full updraught computation. Once the final cloud base mass flux $M_{u,b}^n$ is obtained all the mass fluxes and detrainment rates from the initial updraught computation are scaled by a factor $M_{u,b}^n / M_{u,b}^{n-1}$.

We still need to specify the convective adjustment time τ. One would expect the adjustment time to be proportional to the life cycle of the cloud and/or the time it takes a gravity wave to propagate through the model grid, i.e. $\tau = \Delta x / \sqrt{gH}$, where Δx is the horizontal model grid spacing, and *H* the depth of the cloud. However, experimentation showed that optimal results in terms of convective adjustment (rainfall) and convection-large-scale interaction are obtained for both the middle latitudes and the tropics using a convective turnover timescale $\tau = H / w_H^u \, \alpha_{res}$, where w_H^u is the cloud averaged updraught velocity, and α_{res} is a factor depending on the horizontal model resolution (α_{res} =1+0.013 Δx*(km)*).

3.3. Closure for shallow convection

Ideally one would like to employ the same closure for deep and shallow convection, e.g. a CAPE closure. Experience shows that this is practical feasible but does not produce optimal results as deep convection occurs in perturbed environments with strong mid-level inflow, and shallow convection is mainly surface driven boundary-layer convection. A closure for shallow convection that aims for an equilibrium of the subcloud layer can be written as

$$\int_{surf}^{base} \frac{\partial \overline{h}}{\partial t} \overline{\rho} dz = 0, \tag{13}$$

where $h = c_p T + Lq + gz$ is the moist static energy. The physical meaning of this equation is simply, what comes in at the surface must come out at the top, i.e. at cloud base. Including all other physical processes, in practice this means taking into account all tendencies of the model produced by other parameterizations, (13) becomes

$$\int_{surf}^{base} \left[-\frac{\partial \left(\overline{w'h'} \right)_{conv}}{\partial z} + \left(\frac{\partial \overline{h}}{\partial t} \right)_{turb} + \left(\frac{\partial \overline{h}}{\partial t} \right)_{dyn} + \left(\frac{\partial \overline{h}}{\partial t} \right)_{rad} \right] \overline{\rho} dz = 0 \tag{14}$$

The surface fluxes are hidden in the tendency for turbulent diffusion $\left(\frac{\partial \overline{h}}{\partial t} \right)_{turb}$. Expressing the convective flux at cloud base by its mass flux formulation

$$\rho \left(\overline{w'h'} \right)_{base}^{conv} = M_b^u \left(h^u - \overline{h} \right)_{base}; \quad \left(\overline{w'h'} \right)_0^{conv} = 0, \tag{15}$$

we obtain the final result for the cloud base mass flux

$$M_b^u = \frac{\int_{surf}^{base} \left[\left(\frac{\partial \overline{h}}{\partial t} \right)_{turb} + \left(\frac{\partial \overline{h}}{\partial t} \right)_{dyn} + \left(\frac{\partial \overline{h}}{\partial t} \right)_{rad} \right] \overline{\rho} dz}{\left(h^u - \overline{h} \right)_{base}} \tag{16}$$

The beauty of this closure is that it adapts automatically to the other physical processes, and to the numerics of the host model. In practice this closure turns out difficult to beat by any closure existing in the literature, e.g. a closure given by αw^* (Grant 2001), where α is an updraught fraction (of order 0.05), and w^* is the convective-scale velocity that is proportional to the surface heat fluxes.

3.4. Numerical solution

The solution of (16) requires that all other physical tendencies are known. It has been shown by Dubal et al. (2004) that for long time integration steps as typically used in models with semi-lagrangian dynamics, a sequential splitting, where the individual physical processes are called sequentially is more accurate than a parallel splitting where all physical processes are called without any updating (interdependence). In the IFS we have implemented the following sequential procedure (Beljaars et al. 2006): After a dynamical time step first the radiation is called, followed by the turbulent diffusion, the convection and finally the cloud scheme. Ideally, we would like to call the convection at last to clean/stabilize the whole column, but as the cloud

scheme requires input from the convection (detrained water), the cloud scheme is actually called twice, once before, and once after the convection. In between each of the physical processes the total physics tendencies are updated, and new intermediate state variables are computed that serve as input for the next physical process. The diffusion, convection, and cloud scheme use each an implicit two-time level implicit solver. The diffusion solver further employs an iterative procedure as the diffusion equation with the diffusion coefficient depending itself on the state variable is non-linear, but a symmetric split implicit/explicit scheme with an implicit step followed by an explicit and a final implicit step could have also been employed.

4. Tracer transport experiments

Examining tracer transport in convective situations allows to visualise, understand, and evaluate convective transport. We compare the tracer transport as simulated with the IFS convection scheme in single-column (SCM) and fully three-dimensional global mode, against corresponding CRM simulations (courtesy J.-P. Chaboureau using the Meso-nh model), and observations. The models are forced with large-scale tendencies for temperature and humidity observed during TOGA-COARE. Furthermore, global simulations are performed for the same period starting from the ERA-40 year reanalysis, using a horizontally uniform tracer fields in order to mimic the absence of horizontal advection in the SCM and CRM.

Figure 4 shows the evolution of the convective and total rainfall rate as produced by the IFS SCM and the CRM. Reassuringly, the IFS convection scheme produces rainfall rates (and therefore also mass fluxes) that are close to the CRM results, so that the comparison of convective tracer transport by the two models is supposed to be meaningful.

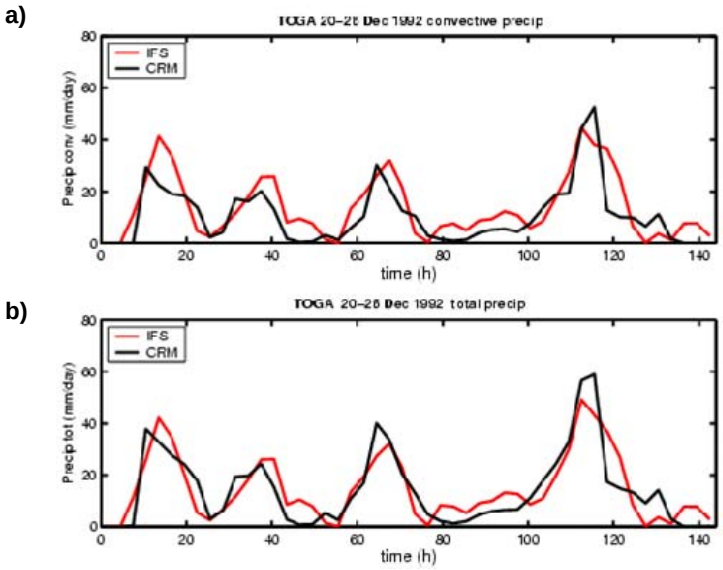

Figure 4. Evolution of convective (a) and total (b) rainfall rate as produced by the IFS SCM and the CRM.

The evolution of a mid-tropospheric tracer as produced by the IFS convection parameterization and the CRM is shown in Figure 5. In both models the mid-tropospheric tracer slowly subsides due to the so called cumulus induced environmental subsidence (see (9)), but the tracer also moves further upward due to updraught transport, and after about 50 h is quickly taken down to the surface by downdraughts. After a period of 3 days the tracer becomes well-mixed, even in the CRM that shows somewhat less mixing the IFS SCM. The IFS global model shows more (realistic) upward transport as the forcing data provided for TOGA-COARE is inaccurate above 14 km producing a too low tropopause.

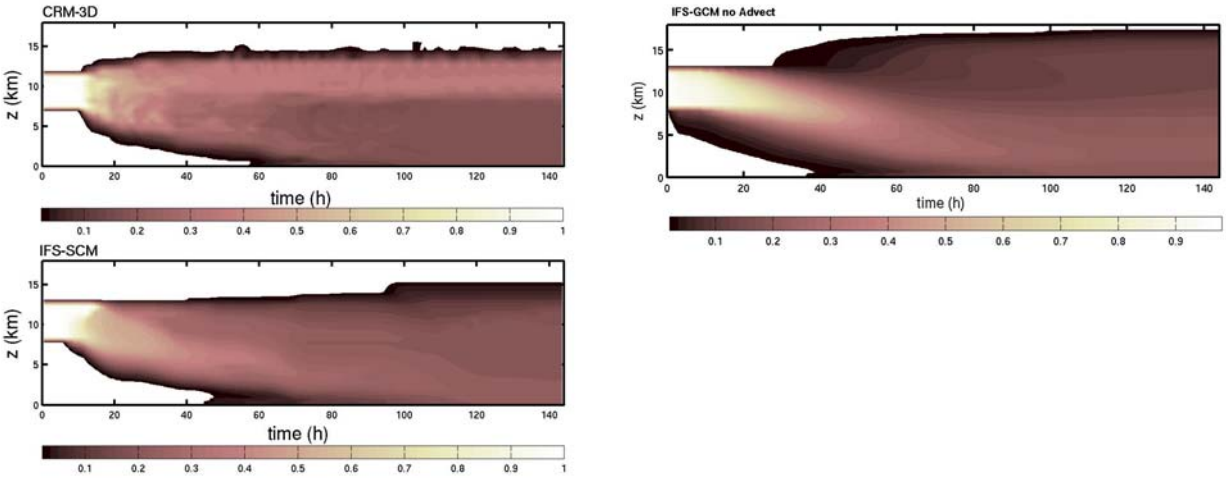

Figure 5. Evolution of a mid-tropospheric tracer during a period of TOGA-COARE as simulated by the IFS SCM, and a three-dimensional CRM (top and bottom left), and the IFS global model for the TOGA-COARE area without horizontal tracer advection.

A useful tool to represent convective mixing/transport is the Mixing Matrix. The dimensions of the matrix is *K x K*, where *K* is the number of model levels, and initially its values are zero apart from the diagonal elements that have value unity. The Mixing Matrix is universal and can be applied to any passive tracer. It is also a useful tool to verify the numerics of the convection scheme as its row values should always sum to one, and neither be negative nor exceed one (monotonicity), and the vertical integral over pressure of its column values must be constant in time (conservation). In Figure 6 it is illustrated for the present case for day 1 and 3 of the integration. Non-zero elements in the upper-left part of the matrix indicate rapid updraught transport, elements just below the diagonal slow subsiding motions, and elements far below the diagonal rapid downdraught transport. After about 3 days the matrix becomes 'full'.

If one wants to perform back-tracing experiments, i.e. to determine the original profile/source of a measured tracer concentration one could invert the mixing matrix. However, after a few time steps this becomes impossible as the matrix becomes singular, indicating that de-mixing is unphysical. The transpose or adjoint of the matrix, however, always exists and is the preferred tool for back-tracing experiments. Further experimentation showed that the adjoint is useful (there is sufficient sensitivity or information) for periods on the order of 12-48h depending on the convective events.

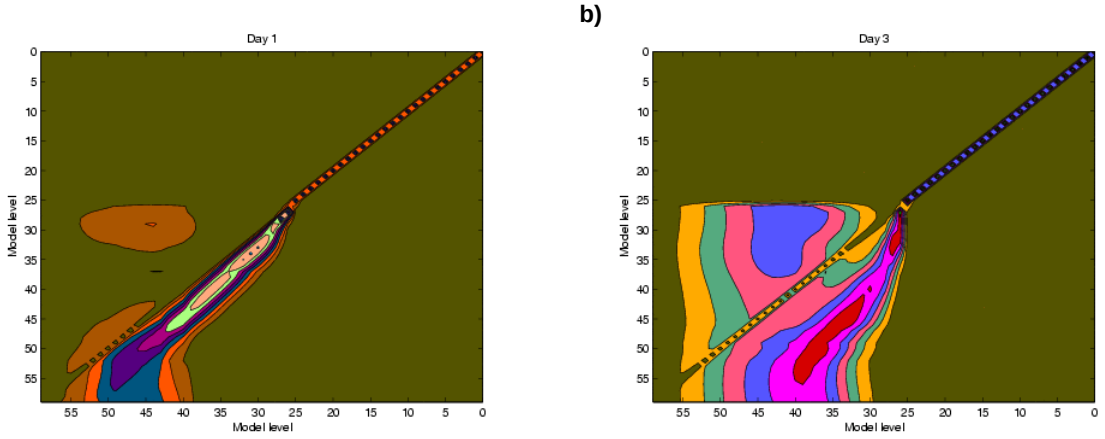

Figure 6. Convective mixing matrix representative for day 1 (a) and day 3 (b) of the integration in a 60-level version of the IFS. The tropopause corresponds to level 25.

As an application to the 'real' atmosphere are shown in Figure 7 profiles of Ozone (a stratospheric tracer) and Carbon Monoxide (a boundary-layer tracer) as measured by routine aircraft over Frankfurt and Chicago. Also are shown results from model studies where the IFS dynamical model has been coupled to the chemical model MOZART[2] in the context of the European Global Monitoring project of the Environment (GMES). The green and red profiles are obtained using the IFS convection and diffusion parametrizations, and the blue profiles correspond to a study where the convective transport has been performed using the MOZART convection scheme. The study generally shows a good correspondence of observed and modeled profiles. However, it also illustrates the importance of the representation of convection, in particular for boundary-layer tracers like the CO, as the results obtained with a different convection scheme seem to be less satisfactory (Figure 7b), and indicative of insufficient upward transport.

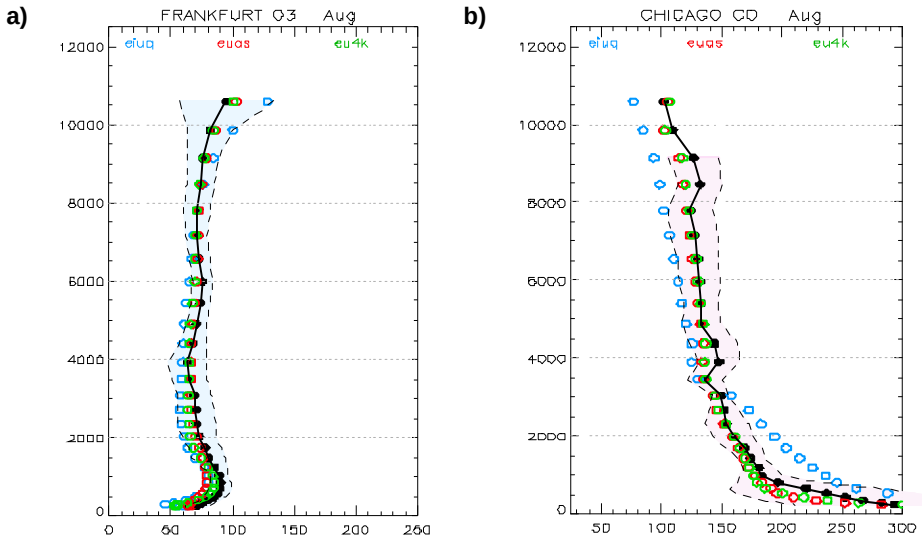

Figure 7. Ozone profiles for Frankfurt (a), and Carbon monoxide profiles for Chicago (b) as measured by passenger aircraft part of the MOZAIC program (black dots), and by the IFS dynamical model coupled to the MOZART chemistry model using the IFS convection scheme (green and red) and the MOZART convection scheme (blue).

5. Tropical convective tendencies and their variability

Globally, the apparent convective tendencies (3) are difficult to observe, some information might be obtained from retrieved latent heating profiles from current satellites like TRMM, Cloudsat/Calipso or SSMI, but we have mainly to rely on the parametrization scheme (here the IFS) or global data from CRMs like the Earth Simulator. Figure 8 shows plots for the Western Pacific mean convective and dynamical tendencies for T, q, u, v, and the corresponding first two Empirical Orthogonal Functions (EOFs).

The EOFs have been added to gain possible information about the variability and modes of the convection. However, one has to be careful with their interpretation as i) they measure the variability related to the 'on' and 'off' state of convection, and also the variability of the (active) convective profiles. A future application of the EOFs could be to compare them to EOFs from CRM data, in order to see if the parametrization can reproduce the variability seen in the CRM, but one could also imagine using EOFs for reduced mode prognostic convection parametrization (Yano et al., 2005).

[2] Currently maintained by Forschungszentrum Jülich

As a summary of Figure 8 we note that in the IFS the average convective heating peaks above the melting level with a heating rate on the order of 5 K/day, whereas for the specific humidity there is drying throughout the troposphere. Above the boundary-layer the dynamics largely balances the convective tendencies (for the temperature radiation is also important) with dynamical cooling and large-scale moistening. The first EOF explains most of the variability seen in the temperature profiles, but less so for the moisture where there is important variability below 600 hPa. Allover, there is more variability in the dynamical tendencies which could be just a signature of synoptic systems, but could also mean (a hypothesis still to be verified) that the convection schemes potentially underestimates variability by producing often a similar profile. The situation for the momentum tendencies is clearly more complicated. One should retain that on average i) the convective momentum transport tends to reduce the vertical shear (is down-gradient) - note that momentum is conserved but not kinetic energy -, that ii) the most important shear regions are the upper- and lower troposphere, troposphere, and iii) that momentum transport by shallow convection is significant. Again there is more variability in the dynamical momentum tendencies, and in particular in the upper troposphere the EOFs of the u component can have both positive and negative sign, whereas for the IFS both EOFs are always positive - which might point to a deficiency in the convective momentum transport at that levels, possibly missing up-gradient transport events.

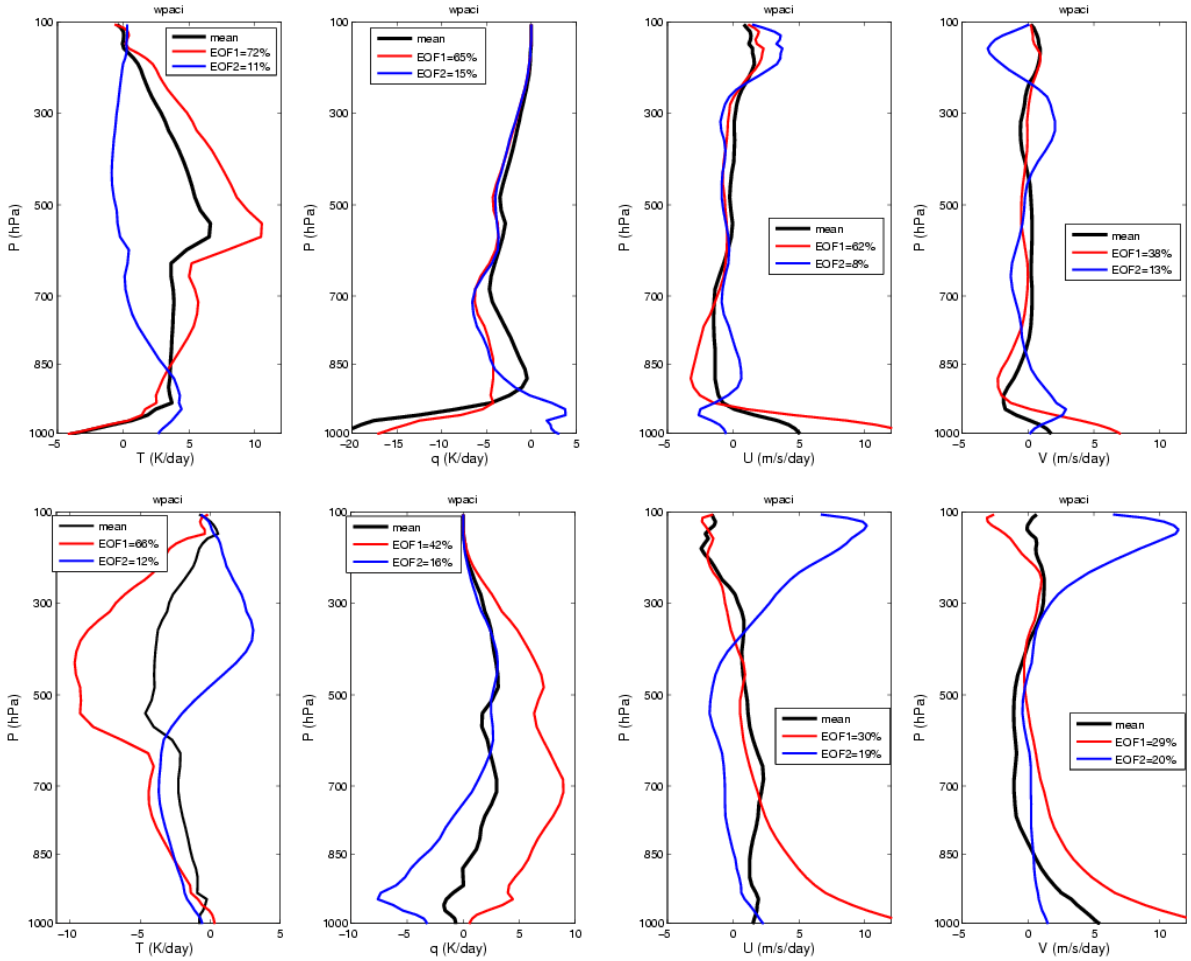

Figure 8. Tendencies of T, q and u, v from the convection (top row), and corresponding dynamical tendencies (bottom row). The bold black lines correspond to the mean tendencies, and the red and blue profiles to the first and second EOF, respectively.

6. Climatology of precipitation and convection

The annual frequencies of occurrence of deep convective clouds (defined as having a thickness exceeding 200 hPa and positive buoyancy) and shallow convective clouds (defined as having some positive buoyancy but having a thickness < 200 hPa) as obtained from the IFS convection parameterization are shown in Figure 9. At first glance the distributions appear realistic with deep convective clouds being a prominent feature of the tropical belt, the storm track regions of the Gulf Stream and the Kuroshio, and the South Pacific and South Atlantic convergence zones, whereas shallow convective clouds are an ubiquitous feature of the subtropical anticyclonic regions, where they are called 'trade wind cumuli'. These statistics are difficult to verify from infrared satellite observations in particular when multi-layered clouds are present. However it could be done now using Cloudsat/Calipso data (see Seminar paper by G. Stephens). A verification for the 'trade wind cumulus' cloud regime using GLAS space lidar data is presented in Figure 10, with the trade cumuli defined as clouds with tops <3 km and cloud cover <0.8 that occur in the subtropical highs as indicated by the pink rectangle in Figure 9b.

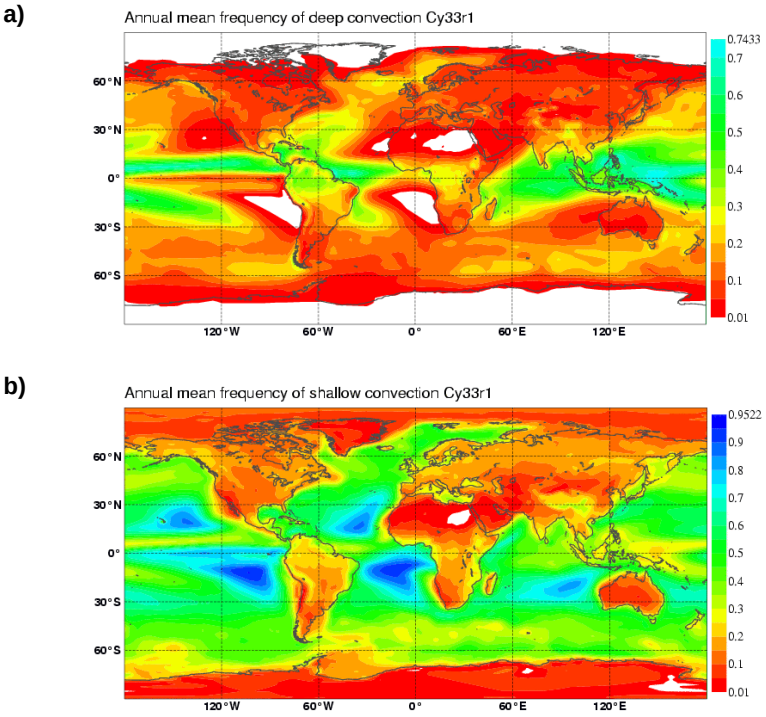

Figure 9. Mean annual frequency of occurence of deep (a) and shallow (b) convective clouds as obtained with IFS Cy33r1.

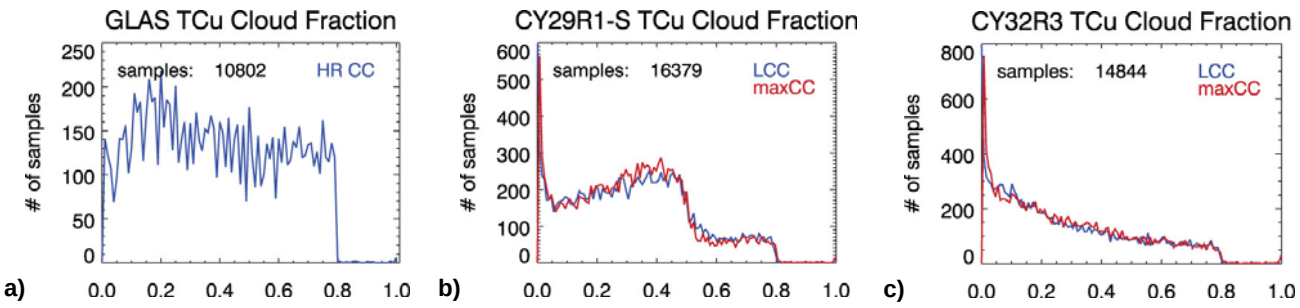

Figure 10. Frequency distribution (not normalized) of cloud cover in the 'trade cumulus regime' defined by clouds in subtropical anticyclones with tops<3 km and cloud cover below 0.8.

The observations show that cloud cover values between 0 and 0.8 are equally likely in the subtropical anticyclones contradicting somewhat the perception of trade wind clouds having low cloud fractions. Model cycles prior to 32r2 tended to produce bimodal distributions, and only since Cy32r3 (November 2007, described above) it is possible to reproduce a continuous quasi-uniform distribution for this cloud regime.

The observed climatological precipitation distribution for the winter months from the GPCP (a merger of raingauge data and infrared satellite derived rain rates) is depicted in Figure 11, together with the corresponding values from seasonal integrations with recent IFS cycles, namely Cy31r1 (operational in 2006) and also used by the ERA-Interim reanalysis, Cy32r2 using the RTTM shortwave radiation code, and the Monte Carlo independent column approximation, and Cy32r3 with revisions to the convection and diffusion (Bechtold et al., 2008). Cy31r1 clearly overestimates precipitation in the Pacific ITCZ and the Indian Ocean, and underestimates precipitation over tropical land. Cy32r2 increases the precipitation in particular over Amazonia by making the clouds more transparent, therefore increasing surface heating and convective activity. Finally, most of the biases are alleviated with the recent Cy32r3 cycle and the following cycle 33r1, by mainly changing the spatial occurrence of the convective precipitation, whereas the global portioning between convective and stratiform precipitation remains essentially unchanged between the model cycles, with 62% of the total global precipitation being of the convective type. Figure 11 illustrates the potential for improvements that modifications to the current convection parametrizations schemes can still provide - for a discussion on the synoptic activity related to the different precipitation fields the reader is referred to the Seminar paper by T. Jung.

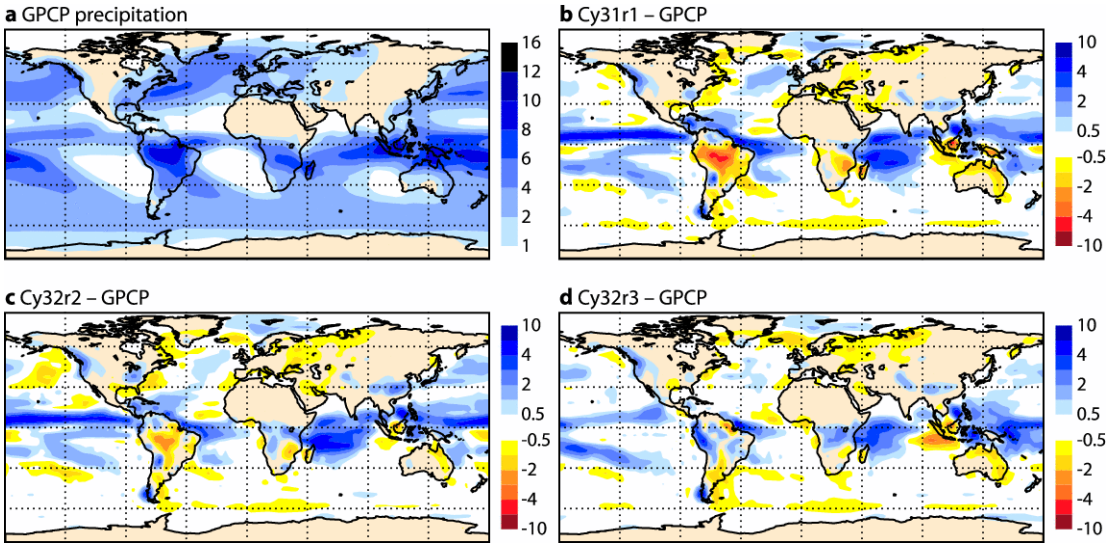

Figure 11. Mean precipitation rates (mm/day) for DJF from the GPCP, and deviation from the GPCP from IFS seasonal integrations with Cy31r1, Cy32r2 and Cy32r3.

7. Diurnal cycle of convection

The diurnal cycle of convection over land is a ubiquitous feature, especially in the tropics, and can be globally assessed using either infrared satellite observations of the OLR (cold cloud tops) or retrievals from the Tropical Rainfall Measurement Mission (TRMM) precipitation radar. As discussed in Yang and Slingo (2001) and also in Bechtold et al. (2004) models using convection parametrizations tend to produce a diurnal cycle of precipitation that occurs too early with respect to observations. We have repeated these exercises with the latest cycle of the IFS, Cy33r1 (June 2008). Observations (Figure 12a) show minimum cloud top temperatures over tropical land that occur in the early evening, whereas minimum cloud top temperatures over the tropical oceans occur during the early morning hours. The model (Figure 12b) reasonably represents

the broad features of the observed phase of the OLR, including the particular coastal regimes of convection off the West coasts of Central America, West Africa and the convection over Indonesia (see also Kikuchi and Wang, 2008). The maximum precipitation in the model (Figure 13) occurs in the early afternoon over land, and between 0 to 4 LST over water. This is 6 to 9 hours earlier than the minimum in the OLR. We know, however, that the daily maximum model rainfall over land occurs still 3h earlier than in the observations. The reason for the apparent discrepancy between a reasonable simulation of the phase of the OLR (clouds) and a 3h phase shift in the simulated maximum rainfall is that the model has a prognostic cloud scheme that represents the gradual thickening of upper-level Cirrus by convective detrainment, whereas the convective precipitation is diagnostic and linked to CAPE which is maximum around noon, just prior to the onset of precipitation.

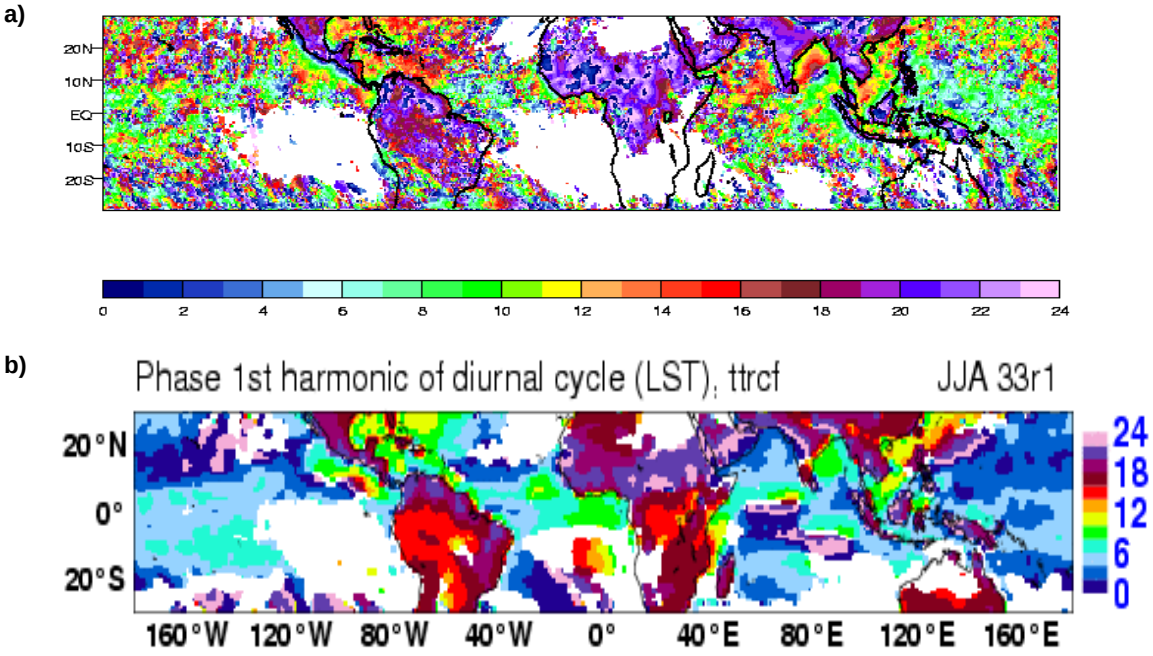

Figure 12. Global map showing phase (LST) when satellite observed brightness temperature is minimum for JJA, or more precisely when the first diurnal harmonics of brightness temperature is minimum. (a), after Yang and Slingo (2001), and (b) cloudy part of the Outgoing Longwave Radiation as obtained from a 4-member ensemble of seasonal T159 integrations with IFS cycle 33r1.

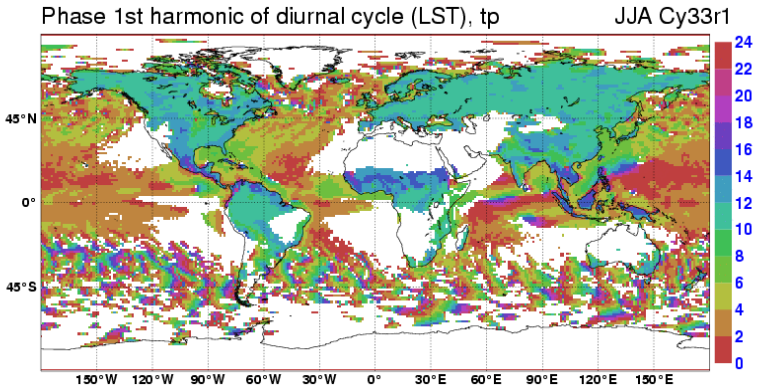

Figure 13. Same as Figure 12, but for the total surface precipitation of the model. Note that there is no distinct diurnal signal in the northern and southern hemispheres storm tracks.

However, our ultimate goal is to perform a quasi-real time verification of clouds and convection using exactly comparable products, namely the Meteosat 9 brightness temperatures (BTs) in the 10.8µ window channel and the corresponding simulated BTs from the high-resolution (currently T799) operational forecast. A first preliminary comparison is presented in Figure 14 for the period 22 August to 3 September 2008, indicating i) that the spatial distribution of the BTs (cloud field) is very similar in the observations and the 24-48h forecasts, but with a narrower extension in the model over tropical Africa, ii) there is no clear diurnal signal in the middle latitudes, and iii) distinctive convective regimes can be identified over tropical Africa, including coastal convection, and convection over the mountainous regions of Tchad and Ethiopia that tends to precede the convection further west by a few hours.

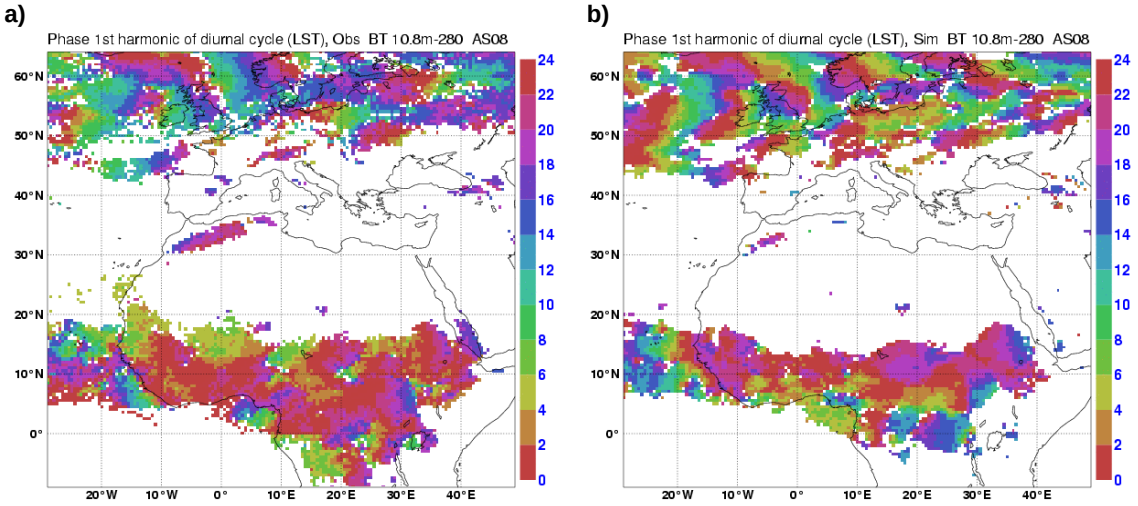

Figure 14. Phase (LST) of the first harmonic of the diurnal cycle of BTs in the infrared 10.8µ channel as observed by Meteosat 9 (a), and from the operational T799 24-48h forecasts for the period 22 August - 3 September 2008. A 280 K mask has been applied to the averaged data in order to eliminate the strong clear sky(hot) surface signal, and to retain only the cloud/convection signal.

8. Forecasts of mesoscale convective systems

In this section we want to address the question if the convection parametrization is able to produce realistic coherent and propagating mesoscale convective systems. As in the previous section the focus is on the North-West African monsoon region, where large mesoscale convective systems, so called squall lines, form south of the African easterly jet and propagate westward. The meteorology of this region has been thoroughly studied during the AMMA 2006 field campaign (Redelsperger et al., 2006), and recently a reanalysis has been made available by ECMWF at resolution T511 (40 km) that includes most of the observations collected during the campaign (Augusti-Panareda et al. 2008).

Several short-range, 48 h re-forecasts have been carried out for this period at resolutions T511, but also at T1279 (15 km, which will become the operational resolution in 2009) that are initialised with the special AMMA reanalysis, and use the latest IFS model cycle 33r1. Furthermore, we also compare the forecasts to limited domain simulations with the Meso-nh (Lafore et al., 1998) CRM at resolution 5 km that use the reanalysis as initial and boundary conditions. The CRM has been run without a parametrization for deep convection, but still uses parametrizations for shallow convection and subgrid-cloudiness as in Söhne et al. (2008). Explicit convection simulations at 5 km resolution are far from ideal, but due to computational constraints (file size, computer time) higher resolutions could not be afforded for the large domain required.

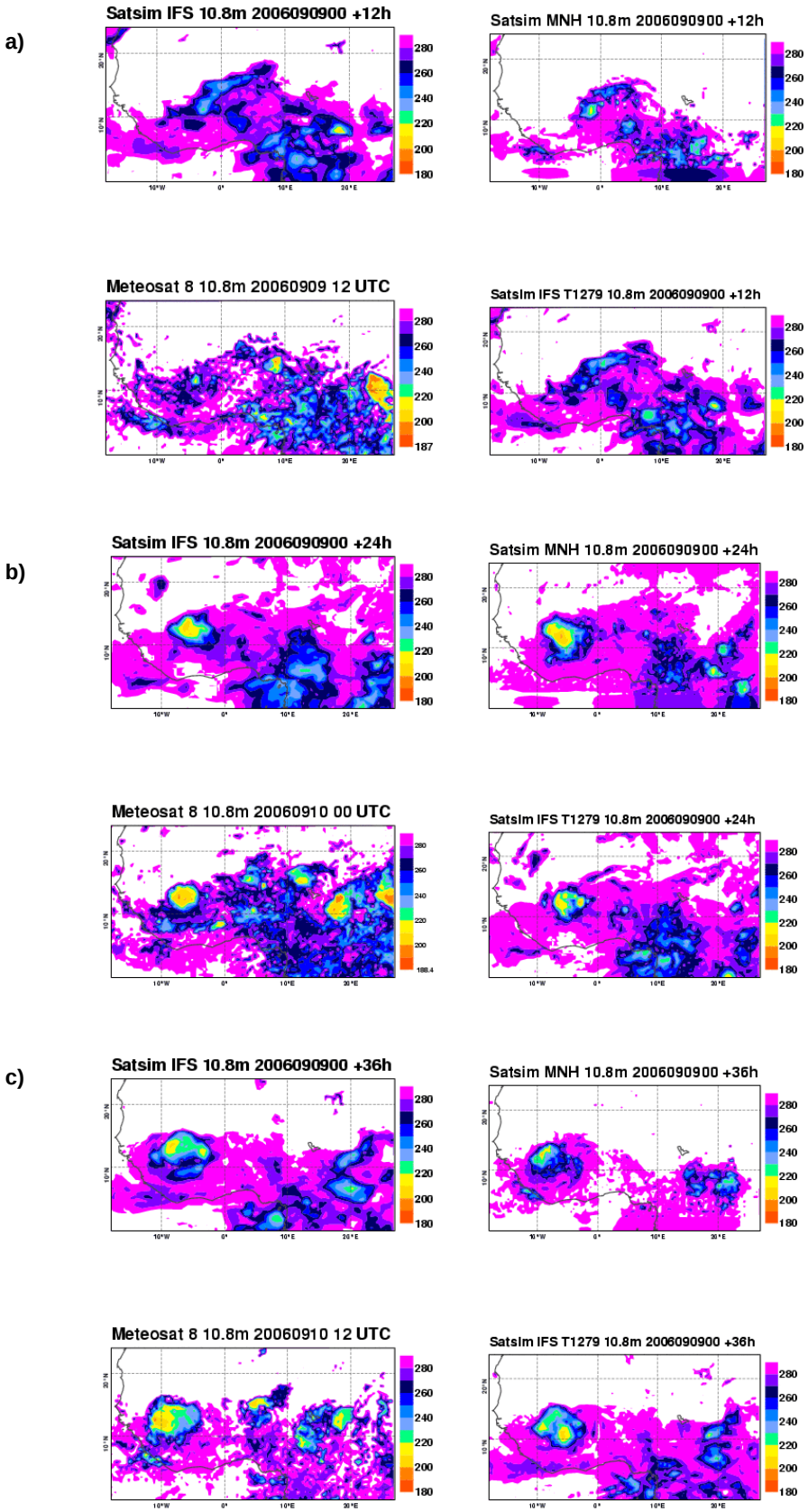

Figure 15. BTs in the 10.8μ window over West Africa as observed by Meteosat 8 9lower left picture in each panel), and simulated by the IFS at resolutions T511, and T1279 (upper left and lower right picture in each panel), and simulated by the Meso-nh model. The simulations are started at 9 September 2006 00 UTC, and results are shown after 12 (a), 24 (b), and 36 h (c) forecast time.

As an example of these simulations, Figure 15 documents the formation and evolution of a squall line system over the Sahel that is associated to an African easterly wave. The domain shown corresponds to the model domain of the CRM. We focus on the square between 0-10°W and 10-20°N. The convective system develops at about 12 h into the forecast, and then quickly grows in size and intensity until 24 h. The location and intensity (cold cloud tops) is comparable in all the forecasts and the observations. At 36 h the system has propagated to 10° W and developed a line structure. Remarkably, the models maintain the system during night and re-strengthen it the following day with the diurnal cycle around noon, but fail to produce smaller convective systems that are apparent in the observations east of 0° W.

More analysis still has to be done including in particular an analysis of the cold pools associated to the squall line, and an analysis of the convective and stratiform heating profiles using EOFs. The momentum fluxes also require further attention, as the momentum fluxes normal to the squall line have to be examined for possible resolved and subgrid-scale up-gradient fluxes, whereas the line parallel fluxes are expected to be downgradient (Zhang and Cho, 1991; Kershaw and Gregory, 1997; Zhang and Wu, 2003). But so far a few preliminary conclusions can already be drawn: The predictability of African squall line systems is higher for systems associated to African easterly waves compared to situations with weaker synoptic forcing. The results seem to be fairly independent of model resolution. This is a good point as the convection parametrization scheme and the physics integration scheme have been designed for this purpose. Unfortunately, no clear benefit seems to be gained by higher resolutions in terms of triggering of convective systems, the 5 km CRM run even tends to underestimate overall convective activity. The models, and in particular also those using convection parametrization can produce signatures of cold pools, and in situations with stronger synoptic forcing can maintain convective systems during the night. The 5 km CRM produces sharper convective frontal structures in the lower levels, but overestimates the upper level mass outflow producing larger wind errors at the 200 hPa level (not shown). Finally, the IFS using a resolved (stratiform) and a subgrid (convective) heating mode can reasonably represent the organization of mesoscale convective systems. Note that the parametrization scheme does not directly contain information on convective organization; one can only make sure that the scheme correctly responds to the large-scale forcing, and hope that the quasi-geostrophic adjustment of the environment to the subgrid diabatic heating produces the right large-scale response and organization.

9. Precipitation and TCW statistics

The last subject I wish to aboard is about precipitation statistics and the relation between precipitation and total column water (TCW). This seems to be somewhat unrelated to what has been presented so far, but provides some insight into the atmosphere as a physical dynamical system, and also constitutes an interesting model verification tool. Figure 16 shows Pdfs of tropical instantaneous precipitation rates, and TCW over the tropical oceans from 0-24 h forecasts with Cy33r1, and corresponding values from the special microwave imager SSMI as retrieved within the 1d-Var system of the assimilation. Similar statistics have been performed by Bretherton et al. (2004). Interestingly, the models Pdf of precipitation rates produces two distinct precipitation regimes, a regime with an exponential slope for moderate precipitation rates from 5 to 50 mm/day, and a power-law distribution for larger precipitation rates that is also present in the retrievals. The SSMI retrievals, however, are only used from model columns were less than 30% of the precipitation rate is in form of ice, and therefore these retrievals have probably excluded the heavy precipitation events and/or very wet model columns (Figure 16b).

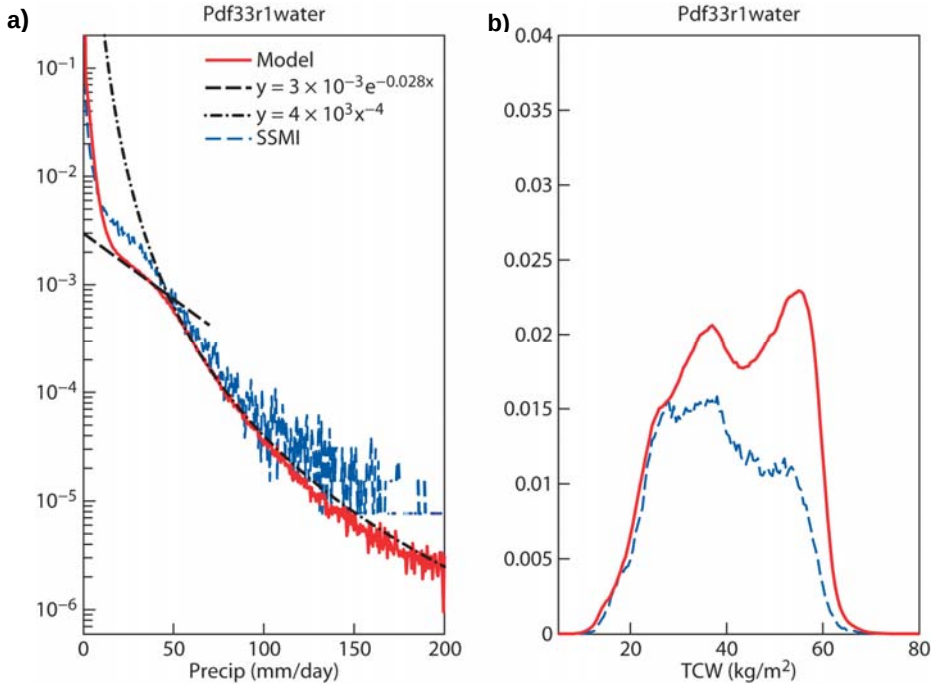

Figure 16. Pdfs of tropical instantaneous precipitation rates (mm/day) (a) and TCW (kg/m2) (b) from 0-24 h T799 operational forecasts with Cy33r1 (red lines), and from SSMI 1D-Var retrievals (blue). Superposed are also exponential and power-law fits to the Pdf of model rain rates.

We can also plot the precipitation rates as a function of the TCW in form of a 2D Pdf, or plot the mean precipitation rate as function of the TCW as illustrated in Figure 17. There is no relationship between the two quantities for TCW contents below 40 kg/m2. However, for values greater than this 'critical' value a nice scaling is observed with a similar slope as in the retrievals. People have claimed (Peters and Neelin, 2006; Neelin et al. 2008) that above this critical value the atmosphere behaves like a self-organized critical system. Prominent members of this group of systems are e.g. forest fires, a cellular automaton, or the simplest model, a sand-pile which continuously receives sand on its top until the slope becomes too steep and the pile collapses, spreading the information (sand) further outside, and so on. Instead of plotting precipitation rate against a dimensional quantity, it is preferable to choose a non-dimensional quantity, and the ideal candidate is the TCW relative humidity or the TCW devided by the vertical integral of saturation mixing ratio (Figure 18). Here the critical point corresponds to a TCW relative humidity of roughly 70 %. The slope in the model data (instantaneous rain rates) is identical to that obtained by Bretherton et al. (2004) but from 24 h averaged SSMI data at resolution T95 (2.5°). However, averaging the model data over a 24 h period produces a slope that is much smaller than that obtained by Bretherton et al. (2004) - in any case it is not desirable averaging model rain rates over long periods as one averages over wet and dry events.

To conclude the discussion we note that the statistical distribution of model rain rates verifies against SSMI, and that the model is able to reproduce the characteristic precipitation regimes of the atmospheric system. We can not confirm yet if the scaling of rain rates against TCW above the critical point is a characteristic of a self-critical system. It is, however, a useful constraint for future data assimilation developments, and also confirms the current assimilation strategy at ECMWF where the information on rain rates from SSMI is converted through 1D-Var retrievals in a TCW increment that is used in the actual 4D-Var assimilation.

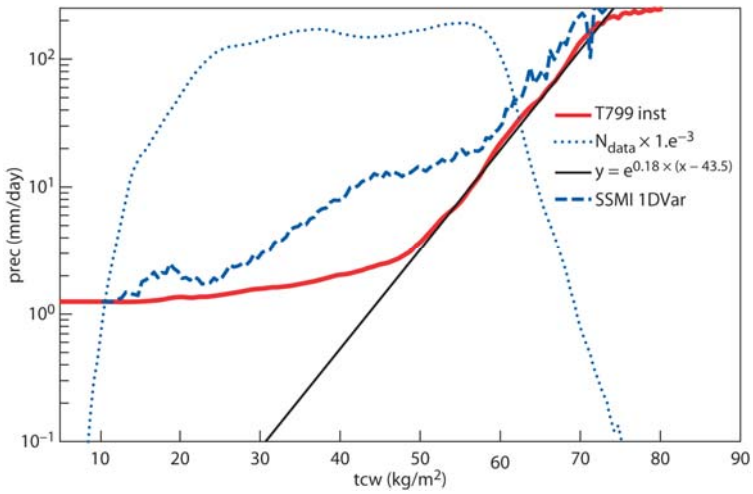

Figure 17. As in Figure 16 but for the mean precipitation rate (mm/day) as a function of TCW. The thin blue dotted line denotes the number of data points in each bin.

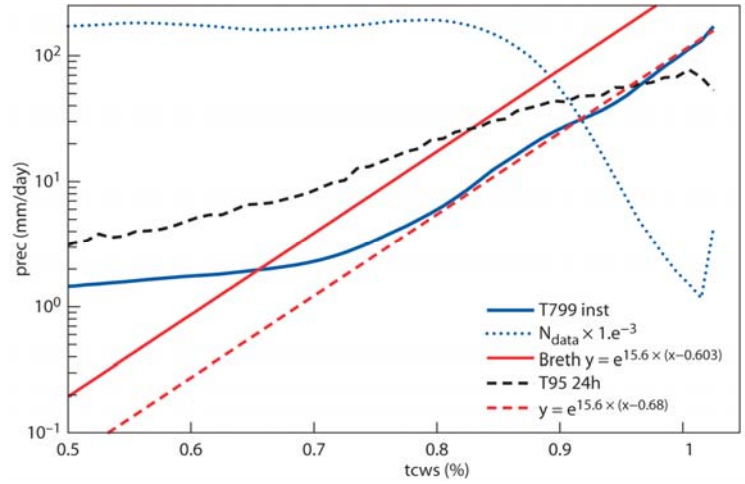

Figure 18 As Figure 17, but for the precipitation rate as a function of the TCW normalized by its saturation value. Here the blue line corresponds to the model data, the red dotted line is a fit to the model data, the solid red line is from SSMI data discussed in Bretherton et al. (2004), and the black dotted line from 24 h accumulated rainfall rates at resolution T95.

10. Summary and Perspectives

We first introduced the contribution of subgrid physical processes on the global energy cycle, and in particular the conversion of convective heating into kinetic energy. The discussion on the parametrization of convection (convective tendencies) within the mass flux framework was limited to a few important issues, namely the entrainment/detrainment, the convective closure or the adjustment process, and numerical issues with the integration of the entire set of physical parametrizations. Application and evaluation of the scheme within the IFS model include single-column model as well as global short-range and seasonal predictions at different horizontal resolutions (15-125 km) with the focus on chemical tracer transport, rainfall and cloud statistics, and the diurnal cycle of clouds and convection. The model results have been compared to observations, analysis, and data from a 3D cloud resolving model.

It is suggested that models using parametrizations for stratiform (resolved) and subgrid (convective) clouds and transport can in principle reproduce i) the observed rainfall spectra, ii) the observed distribution of clouds (e.g. in terms of brightness temperatures), and iii) dynamical mesoscale, synoptic and large-scale features like mesoscale convective systems and convectively-coupled waves (see also article by T. Jung). The obtain optimal and quasi resolution independent results the convection parametrization is required to

respond (trigger and vertical profiles) smoothly to the large-scale forcing, to be sufficiently sensitive to environmental moisture (similar developments/experimentation by Neale and Wu with versions of the NCAR model confirm these results, GEWEX/GCSS meeting Toulouse, 2008[3]), and to represent an adjustment that is scale dependent, but that does not prescribe a strong coupling between the convection and the large-scale (e.g. through the large-scale moisture convergence). Our results showed that still significant progress in the simulation of the mean climate and atmospheric variability can be achieved with improved current parametrizations.

Where are the problems then? Most convection parametrizations are column independent and assume a stationary cloud model, with the consequence that i) they might produce noisy convective (precipitation) fields in space and time, lacking organized structures, the latter might be also due to the lack of spreading cold pools, ii) produce a diurnal cycle of convective rainfall/heating that typically occurs 3 hours earlier than observed, and iii) have difficulties in producing the distinct momentum transport in organized convective systems like squall lines which line-normal is up-gradient and is down-gradient parallel to the line (for a parametrization of these perturbation pressure effects see e.g. Zhang and Cho, 1991; Kershaw and Gregory, 1997; Zhang and Wu, 2003). Also, models with parametrized convection have problems in producing a distinct spectral peak of the Madden-Julian Oscillation in the 45-55 day range.

There have been efforts introducing a memory or time dependence into a convection parametrization, e.g. a prognostic closure as suggested by Pan and Randall (1998) or Scinoccia and Mc Farlane (2004). There has been mixed success with this method, and it has the inconvenience of introducing one additional tunable parameter. It is also not easy to transfer this method to existing parametrizations as they utilize some non-continous trigger mechanism to switch on/off convection. Similar approaches were developed by Piriou (2007), and Gerard and Geleyn (2005), but using the entrainment rate, or the updraught fraction and vertical velocity as prognostic quantities.

Interesting recent developments in 'convection parametrization' in some larger dynamical context have been reported by Kuell et al. (2007) who no longer solve for the convective tendencies inside the mass flux convection scheme, but directly pass the mass perturbation term to the non-hydrostatic host model. So far this approach has only been realised in 2D as it involves numerical problems related to mass conservation. Finally, Yano (2008, communications in preparation) is developing a truncated CRM as a subgrid parametrization under the segmentally constant approximation. The method has the advantage that it takes into account non-hydrostatic pressure effects and under maximum truncation reduces to the single updraught/downdraught mass flux framework.

So what is the future of convection parametrization? During the next 10-20 years the availability and computational speed of global models at O(1 km) resolution will gradually remove the need for deep convection parametrization. But until this can be realised deep convection parametrizations will still be used and useful, not only because they provide a simple and efficient filtering (instabilities, noise) and control of the forecasts. Shallow convection parametrization will remain necessary for the foreseeable future. Then, during the next decade or so should we go for a more prognostic description of convection, for more (microphysical) complex schemes, or for a prognostic reduced mode or fitting approach using EOFs and/or neural networks? This question cannot be answered as its answer should be based on try and see. For a numerical weather prediction centre like ECMWF, however, simplicity and quasi linearity is important, especially in the context of variational data assimilation where the tangent-linear model (convection) code

[3] http://www.knmi.nl/~siebesma/PAN-GCSS/presentations.html

must be a good approximation of the non-linear model. We still aim for, however, for an improved communication between neighbouring convective grid columns.

Acknowledgements

My gratitude goes to my colleagues Mike Ahlgrimm, Anton Beljaars, Jean-Pierre Chaboureau, Johannes Flemming, Alain Geer, Thomas Jung, Martin Köhler, Fernando Li, Philippe Lopez, Jean-Jaques Morcrette and Andrew Orr for their help in preparing this material, and to Martin Miller and Philippe Bougeault for many helpful discussions.

References

Agusti-Panareda and many co-authors, 2008: Radiosonde humidity bias correction for the West African region for the special AMMA reanalysis at ECMWF. *Quart. J. Roy. Meteor. Soc.,* submitted.

Arakawa, A. and W. Schubert, 1974: Interaction of a cumulus ensemble with the large-scale environment. Part I. *J. Atmos. Sci.,* **31,** 674-701.

Arakawa, A., 2004: The cumulus parameterization problem: Past, present, and future. *J. Climate,* **17,** 2493-2525.

Bechtold, P., J.-P. Chaboureau, A. Beljaars, A. K. Betts, M. Köhler, M. Miller and J.-L. Redelsperger, 2004: The simulation of the diurnal cycle of convective precipitation over land in a global model. *Quart. J. Roy. Meteor. Soc.,* **130,** 3119-3137.

Bechtold, P., M. Köhler, T. Jung, F. Doblas-Reyes, M. Leutbecher, M. Rodwell, F. Vitart and G. Balsamo, 2008: Advances in simulating atmospheric variability with the ECMWF model: From synoptic to decadal time-scales. *Quart. J. Roy. Meteor. Soc.*, **134,** 1337-1351. Also available as *ECMWF Technical Memorandum* **No 556**.

Beljaars, A. C. M., P. Bechtold, M. Köhler, J.-J. Morcrette, A. M. Tompkins, P. Viterbo and N. Wedi, 2004 : The numerics of physical parameterization : in ECMWF Seminar proceedings on « Recent developments in numerical methods for atmosphere and ocean modelling » pp. 113-134.

Bjerknes, J., 1938: Saturated ascent of air through a dry-adiabatically descending environment. *Quart. J. Roy. Meteor. Soc.,* **64,** 325-330.

Bretherton, C. S., M. Peters and L. E. Back, 2004: Relationships between water vapor path and precipitation over the tropical oceans. *J. Climate,* **17,** 1517-1528.

Dubal, M., N. Wood and A. Staniforth, 2004: Analysis of parallel versus sequential splittings for time-stepping physical parametrizations. *Mon. Wea. Rev.,* **132,** 121-132.

Gerard, L. and J.-F. Geleyn, 2005: Evolution of a subgrid deep convection parametrization in a limited area model with increasing resolution. *Quart. J. Roy. Meteor. Soc.,* **131,** 2293-2312.

Grant, A. L. M., 2001: Cloud-base fluxes in the cumulus-capped boundary layer. *Quart. J. Roy. Meteor. Soc.,* **127,** 407-422.

Gregory, D. and M. Miller, 1989: A numerical study of the parameterization of deep tropical convection. *Quart. J. Roy. Meteor. Soc.,* **115,** 1209-1241.

Kuell, V., A. Gassmann and A. Bott, 2007: Towards a new hybrid cumulus parametrization scheme for use in non-hydrostatic weather prediction models. *Quart. J. Roy. Meteor. Soc.,* **133,** 479-490.

Kuo, H. L., 1965: On the formation and intensification of tropical cyclones through latent heat release by cumulus convection. *J. Atmos. Sci.,* **22,** 40-63.

Lin, C. and A. Arakawa, 1997: The macroscopic entrainment processes of simulated cumulus ensemble. Part II: Testing the entraining-plume model. *J. Atmos. Sci.,* **54**, 1044-1053.

Lafore, J.-P., and many co-authors, 1998: The Meso-NH atmospheric simulation system. Part I: Adiabatic formulation and control simulations. Scientific objectives and experimental design. *Ann. Geophys., **16,*** 90-109.

Piriou, J.-M., J.-L. Redelsperger, J.-F. Geleyn, J.-P. Lafore and F. Guichard, 2007: An approach for convective parameterization with memory: Separating microphysics and transport in grid-scale equations. *J. Atmos. Sci.,* **64,** 4127-4139.

Kershaw, R. and D. Gregory, 1997: Parameterization of momentum transports by convection. I: Theory and cloud modeling results. *Quart. J. Roy. Meteor. Soc.,* **123,** 1133-1151.

Kikuchi, K., and B. Wang, 2008. Diurnal precipitation regimes in the global tropics. *J. Climate,* **21,** 2680-2696.

Manabe, S. and R. Strickler, 1964: Thermal equilibrium of the atmosphere with a convective adjustment scheme. *J. Atmos. Sci.,* **21,** 361-385.

Neelin, J. D., O. Peters and K. Hales, 2008: The transition to strong convection. *J. Atmos. Sci.* submitted.

Peters, O. and J. D. Neelin, 2006: Critical phenomena in atmospheric precipitation. Nature (Physics), published online doi:10.1038/nphys314.

Redelsperger, J.-L., D. B. Parsons and F. Guichard, 2002: Recovery processes and factors limiting cloud-top height following the arrival of a dry intrusion observed during TOGA COARE. *J. Atmos. Sci.,* 59, 2438-2457.

Redelsperger J.-L., C. D. Thorncroft , A. Diedhiou, T. Lebel, D. J. Parker, and J. Polcher, 2006: African Monsoon Multidisciplinary Analysis. *Bull. Am. Meteorol. Soc.,* **86,** 1739-1746.

Söhne, N. J.-P. Chaboureau and F. Guichard, 2008: Verification of cloud cover forecast with satellite observation over West Africa. *Mon. Wea. Rev.,* **136,** to appear.

Steinheimer, M., M. Hantel and P. Bechtold, 2008: Convection in Lorenz's global energy cycle with the ECMWF model. *Tellus,* **60A**, 1001-1020. Also available as *ECMWF Technical Memorandum* **No 545**.

Wood, N., M. Diamantakis and A. Staniforth, 2007: A monotonically-damping second-order-accurate unconditionally-stable numerical scheme for diffusion. *Quart. J. Roy. Meteor. Soc.,* **133,** 1559-1572.

Yanai, M., S. Esbensen and J. Chu, 1973: Determination of bulk properties of tropical cloud clusters from large-scale heat and moisture budgets. *J. Atmos. Sci.,* **30,** 611-627.

Yang, G.-Y. and J. Slingo, 2001: The diurnal cycle in the tropics. *Mon. Wea. Rev.,* **129,** 784-801.

Yano, J.-I., J.-L. Redelsperger, P. Bechtold and F. Guichard, 2005: Mode decomposition as a methodology for developing convective-scale representations in global models. *Quart. J. Roy. Meteor. Soc.,* **131,** 2313-2336.

Zhang, G. J. and H.-R. Cho, 1991: Parameterization of the vertical transport of momentum by cumulus clouds. Part I: Theory. *J. Atmos. Sci.,* **48,** 1483-2539.

Zhang, G. J. and X. Wu, 2003: Convective momentum transport and perturbation pressure field from a cloud-resolving model simulation. *J. Atmos. Sci.,* **60,** 1120-1139